PROCEEDINGS OF SPIE

Additive manufactured x-ray optics for astronomy

Carolyn Atkins, Charlotte Feldman, David Brooks, Stephen Watson, William Cochrane, et al.

SPIE.

Additive manufactured X-ray optics for astronomy

Carolyn Atkins*[a], Charlotte Feldman[b], David Brooks[c], Stephen Watson[a], William Cochrane[a],
Melanie Roulet[a,d], Peter Doel[c], Richard Willingale[b] and Emmanuel Hugot[d]

[a]UK Astronomy Technology Centre, Royal Observatory, Edinburgh, EH9 3HJ, UK
[b]University of Leicester, Department of Physics and Astronomy, Leicester, LE1 7RH, UK
[c]University College London, Department of Physics and Astronomy, London, WC1E 6BT, UK
[d]Aix Marseille Univ, CNRS, Laboratoire d'Astrophysique de Marseille, Marseille, France

ABSTRACT

Additive manufacturing, more commonly known as 3D printing, has become a commercially established technology for rapid prototyping and the fabrication of bespoke intricate parts. Optical components, such as mirrors and lenses, are now being fabricated via additive manufacturing, where the printed substrate is polished in a post-processing step. One application of additively manufactured optics could be within the astronomical X-ray community, where there is a growing need to demonstrate thin, lightweight, high precision optics for a *beyond Chandra* style mission.

This paper will follow a proof-of-concept investigation, sponsored by the UK Space Agency's National Space Technology Programme, into the feasibility of applying additive manufacturing in the production of thin, lightweight, precision X-ray optics for astronomy. One of the benefits of additive manufacturing is the ability to construct intricate lightweighting, which can be optimised to minimise weight while ensuring rigidity. This concept of optimised lightweighting will be applied to a series of polished additively manufactured test samples and experimental data from these samples, including an assessment of the optical quality and the magnitude of any print-through, will be presented. In addition, the finite element analysis optimisations of the lightweighting development will be discussed.

Keywords: additive manufacturing, x-ray optics, finite element analysis, lightweighting, x-ray telescope, topology optimisation

1. INTRODUCTION

Outlined within this paper is a program of study, funded by the UK Space Agency's (UKSA) National Space Technology Programme, investigating the application of additive manufacturing (AM) towards space-based optics and astronomical X-ray optics in particular. The rational behind this research is that future X-ray observatories, such as the NASA concept study *Lynx*,[1] will require a batch production of high spatial resolution lightweight optical components. AM is an ideal technology for batch production with the capability to build (print) several optical components simultaneously; however, questions remain as to the ability to polish the printed substrate, the magnitude of lightweighting that can be achieved and how these might impact upon the optical performance. The UKSA project has both an experimental and a theoretical theme. The experimental theme investigates the optical polishing of a number of commercially available AM substrates and uses the finite element analysis (FEA) tool, topology optimisation, to optimise the lightweighting structure to minimise the polishing print-through effect - this theme is presented herein. The theoretical theme simulates an AM X-ray reflecting prototype system, via ray-tracing, to provide a representative description of the system performance, the conclusion of this theme will be a prototype system that can be fabricated and X-ray tested in the future - this research is described in the paper by *C. Feldman et al.*,[2] which was also presented at this conference.

Creating reflective surfaces on AM substrates has become an active area of research[3,4] and the ready ability to lightweight makes AM very appealing where a system is bounded by weight constraints, for example in space-based applications. In the paper by *Sweeney et al.*,[3] a concave aluminium mirror was fabricated with a form

---

*Email: carolyn.atkins@stfc.ac.uk

error of $< 1\lambda$ ($\lambda = 633nm$) and a surface roughness between 6-8nm root mean square (rms) after diamond turning. A further improvement in form error and roughness was achieved via robotic polishing. In the paper by *Herzog et al.*[4] two samples were created in aluminium and titanium; an optical surface was not obtained on the titanium, but the aluminium sample was polished to a surface roughness of 22nm rms. These examples highlight a potential for AM to be applied to optics manufacture although further investigation is required to push the optical surface to precision and high precision quality (surface roughness $< 2nm$ and $< 0.5nm$ rms respectively - rule of thumb).

The experimental theme of the UKSA project required the use of commercially available AM facilities in order to reduce the lead time between fabrication and polish. In addition, multiple materials and methods were trialled in order to prevent potential bias towards a single material/method as alternative printing methods may have an advantage - for example the liquid based stereolithography process provides a smoother surface post-build than the so far tested metal laser sintering process. The polishing of the samples was performed at University College London's Optical Science Laboratory (OSL), OSL has prior experience in polishing AM materials and therefore their expertise was particularly beneficial.

Two sets of lightweighted samples were fabricated, the first samples investigated the ability to create a reflective surface using a range of the AM materials. The second samples down selected on material choice and featured an optimised lightweighted design created via the finite element analysis (FEA) tool topology optimisation, where the structure was optimised to minimise the polishing print-through effects.

2. INITIAL SAMPLE DESIGN AND MANUFACTURE

2.1 First sample design

There were three considerations in the design of the first set of samples:

1. To minimise print-through/quilting from the polishing process.

2. A design that is not traditionally used in optical lightweighting.

3. A optical prescription and dimensions that were quick to polish and measure.

The design shown in Figure 1 was selected; the arches design of lightweighting was chosen due to its historic use in structural design and a flat optical prescription was chosen for ease of polishing and metrology. The diameter of the part was 40mm, with a 4mm thickness of lightweighting and 1mm thick substrates to sandwich the lightweighting. This design is analogous to the sandwich mirror structure, which is often used in traditional lightweighted mirrors, where a mirror can be lightweighted to between $20\% \rightarrow 40\%$ of its original mass.[5] Fabrication of these traditional sandwich mirrors is relatively expensive and technically difficult, therefore to print a sandwich mirror directly has distinct advantages.
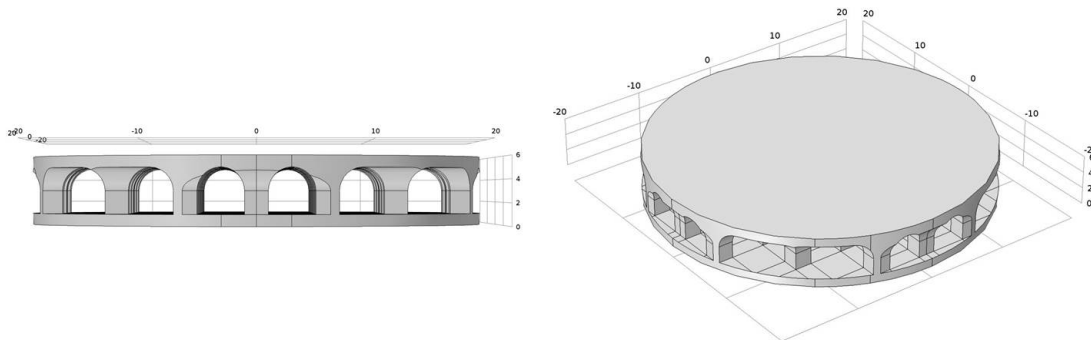

Figure 1. Schematic of the initial sample design: 40mm diameter, 6mm in height

The samples were fabricated at CA Models; a company local to the UK Astronomy Technology Centre in Edinburgh. CA Models have a variety of AM machines, they print primarily in plastics, but have aluminium capability. The advantage of a local company was the ability to visit the facility and to gain insight into the practical process of printing. The selected materials, based on machine type diversity and optimum material properties, and their corresponding post-processing details are presented in Table 1.

Table 1. Selected materials and post-processing

Sample #	Substrate material	Printing method	Post-process
1	Bluestone	Stereolithography	Electroplated nickel coating
2	Glass filled nylon	Selective Laser Sintering	Electroplated nickel coating
3	$AlSi_{10}Mg$	Metal Laser Sintering	CNC milled
4	$AlSi_{10}Mg$	Metal Laser Sintering	CNC milled + electroless nickel coating

For this proof of concept research, there was a desire to trial unconventional materials and processes. Previous research had demonstrated that optical surfaces could be created using metal laser sintering; however, to the author's knowledge neither stereolithography or selective laser sintering in plastics had been trialled for the production of mirrored surfaces. The mechanical properties of the printed materials are listed in Table 2. It is immediately evident that is terms of coefficient of thermal expansion (CTE) and Young's modulus that the nominally plastic materials of Bluestone and glass filled nylon are far from desirable; however, the aim was to trial new materials and processes in preparation for what might be possible with improved future capability/materials.

Table 2. Physical properties of the selected materials - values taken the CA Models data sheets[6, 7]

Material	Density [g/cm^3]	Young's modulus [GPa]	CTE [$\times 10^{-6}/°C$]
Bluestone	1.78	7.6	33-44
Glass filled nylon	1.23-1.28	3.2	68
$AlSi_{10}Mg$	2.7	64	21^a

^{a} *Value taken from an alternative printed $AlSi_{10}Mg$ data sheet*

2.2 Metrology post fabrication

Multiple samples were produced out of each process to investigate the quality of the printing process and to quantify the magnitude of post-processing required. Due to the rough surface post-build a contact profilometer was used to assess each sample surface. Three orientations were measured: 0°, 45° and 90°, the 0° and 90° orientations are defined using Figure 1 as being from $-20mm \rightarrow 20mm$ in x and y axes respectively with the disk is in the x, y plane. The profiles from the three raw prints (i.e. immediately removed from the printer) in the 0° orientation are shown in Figure 2. The Bluestone profile (upper plot) highlights a periodic structure with approximately the same spatial frequency as the arches lightweighting structure beneath. The sample is smooth with small regular indentations, which are a result of a cracked scum layer which has dried upon the Bluestone substrate after rinsing with iso-propanol to remove excess resin - this scum layer is easily removed leaving a smooth surface below. Using Fourier filters to remove the low- to mid-order spatial frequencies with cut-offs at 2.5mm and 0.8mm, the rms roughness (Rq) of the Bluestone sample was $\sim 4.26\mu m$ and $\sim 3.76\mu m$ respectively averaging all orientations.

The middle plot shows the raw glass filled nylon sample, this sample exhibited the roughest surface at $\sim 17.09\mu m$ Rq for 2.5mm cut-off and $\sim 13.65\mu m$ Rq for 0.8mm cut-off. Unlike the Bluestone sample, no periodic features were visually apparent. The raw aluminium print is shown in the bottom plot. The profile demonstrates a periodic structure with roughly the same spatial frequency as the underlying lightweighting structure; however the form of the periodicity is different to that observed in the Bluestone sample - considering the difference in fabrication method this is not unexpected. The Rq of the aluminium sample is $\sim 12.16\mu m$ for 2.5mm cut-off and $\sim 8.91\mu m$ for the 0.8mm cut-off.

A Fourier analysis of each orientation of the three raw post-print samples is shown in Figure 3. The Bluestone sample (upper plot) highlights the print-through of the lightweighting structure from fabrication in all axes. In
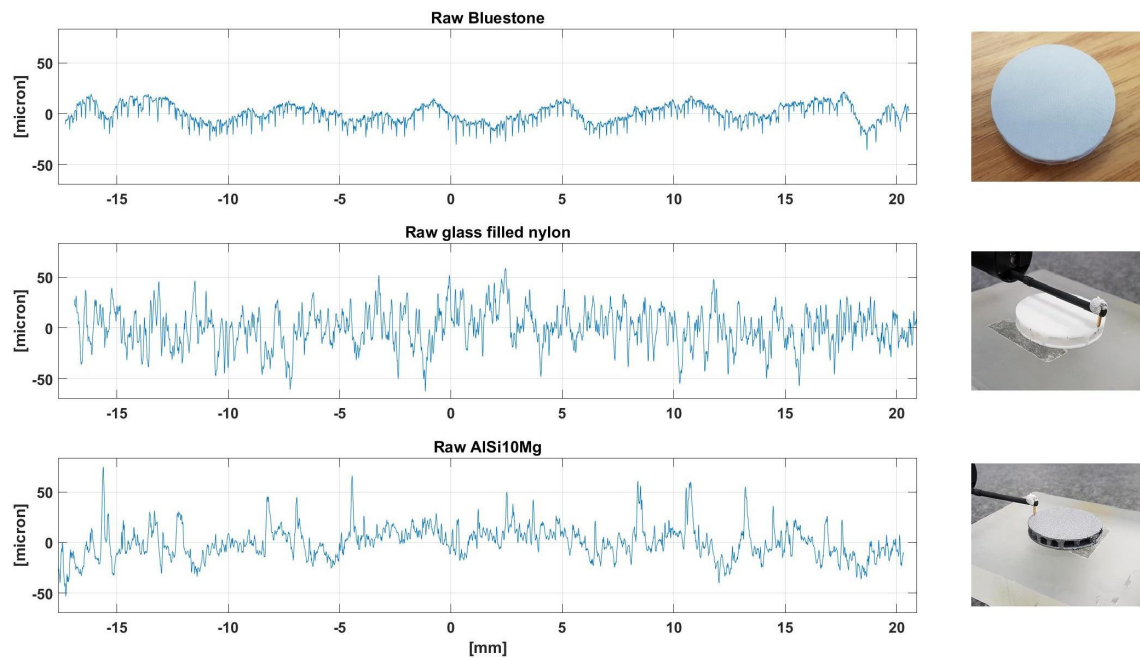
Figure 2. Form Talysurf Intra data taken from the raw printed samples: Bluestone (top), glass filled nylon (middle) and aluminium (bottom).
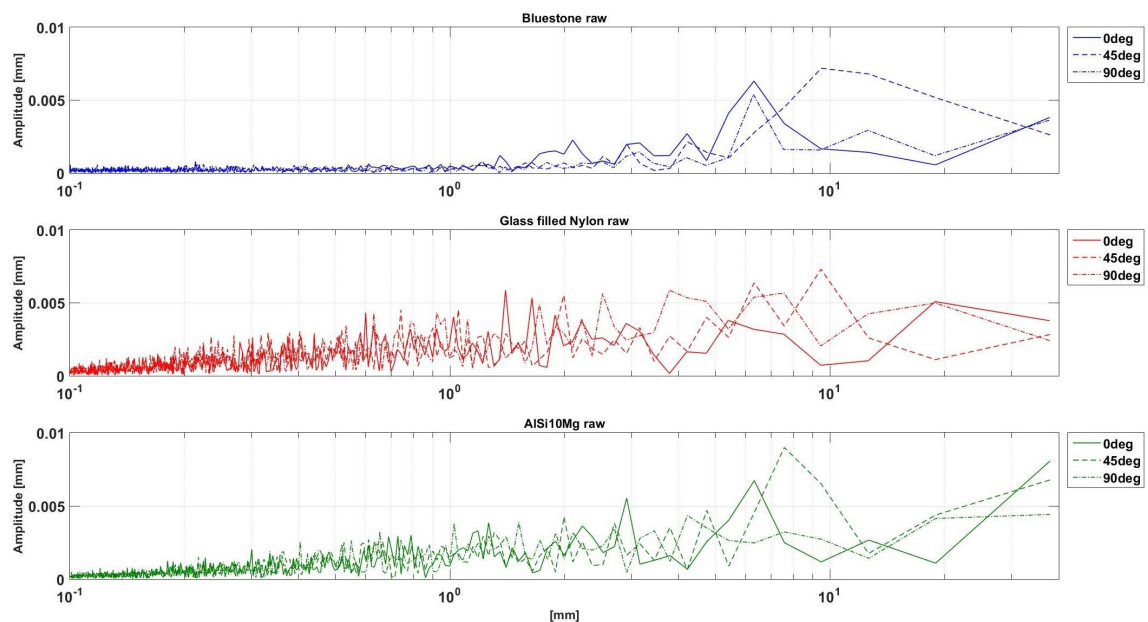

Figure 3. A Fourier analysis of the Talysurf Intra profilometry data highlighting the three orientations for each sample: Bluestone (top), glass filled nylon (middle) and aluminium (bottom).
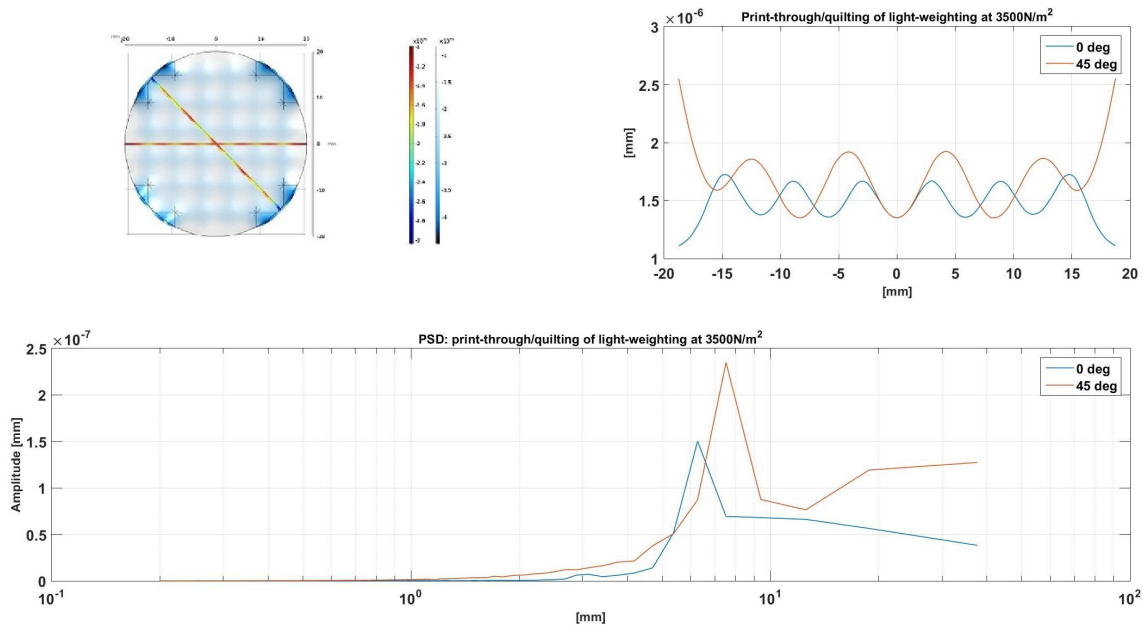
Figure 4. *Upper left*: an FEA simulation highlighting the anticipated polishing deformations, *upper right* line profiles taken from the simulation matching the measurement orientations of the profiler and the *lower* plot demonstrates a Fourier analysis of the profiles.

the $0°$ and $90°$ data a dominant peak is shown at $\sim 6.3mm$, whereas in the $45°$ data the peak is shifted to $\sim 9.5mm$, which is expected considering the measurement is now taken over the diagonal of a grid. An FEA simulation of the design was performed by modelling an applied load upon the optical surface and investigating the distortion caused by the lightweighting upon the optical surface. A Fourier analysis of the $0°$ and $45°$ simulated line profiles is shown in Figure 4 and it illustrates the expected shift in dominant spatial frequency from $0°$ to $45°$ - only the form rather than the magnitude of displacement was of interest for this analysis.

The raw aluminium profile (bottom plot) highlights a frequency peak in both the $0°$ and $45°$ orientations, but not in the $90°$ orientation. The location of the peaks are $\sim 6.3mm$ and $\sim 7.6mm$ for the $0°$ and $45°$ orientations respectively, which again is in-line with the FEA simulation in Figure 4. It is known in the Bluestone and aluminium samples that the building direction of the part is in the $0°$ direction, which indicates that the orientation of the part within the machine has some influence on the observed print-through. The glass filled nylon sample does not appear to have any dominant spatial frequencies associated with a print-through of the underlying lightweighting upon the optical surface.

2.3 Samples prior to polish

Figure 5 highlights the four samples prior to polish. The glass filled nylon and the Bluestone samples were both encapsulated in $100\mu m$ pure Ni via electroplating. Due to the non-uniform nature of electrodeposition,[8] which results in edges and corners being plated preferentially, both of the surfaces prior to polishing exhibited a concave form of $\sim 50\mu m$ peak-to-valley (PV). The mimicry of electrodeposition caused the periodic structure observed in the Bluestone sample in Figure 2 to be replicated in Ni coating. One aluminium sample had no coating and the only post-processing prior to polish was CNC machining to smooth the surface. The second aluminium part was machined and then coated in electroless Ni (nickel phosphor - NiP); the catalytic coating process ensured a uniform thickness of $100\mu m$.

3. POLISHING AND METROLOGY

The Optical Science Laboratory (OSL) at University College London was responsible for the grinding and polishing of the four samples. The grinding process used silicon carbide to prepare the surfaces for polish and
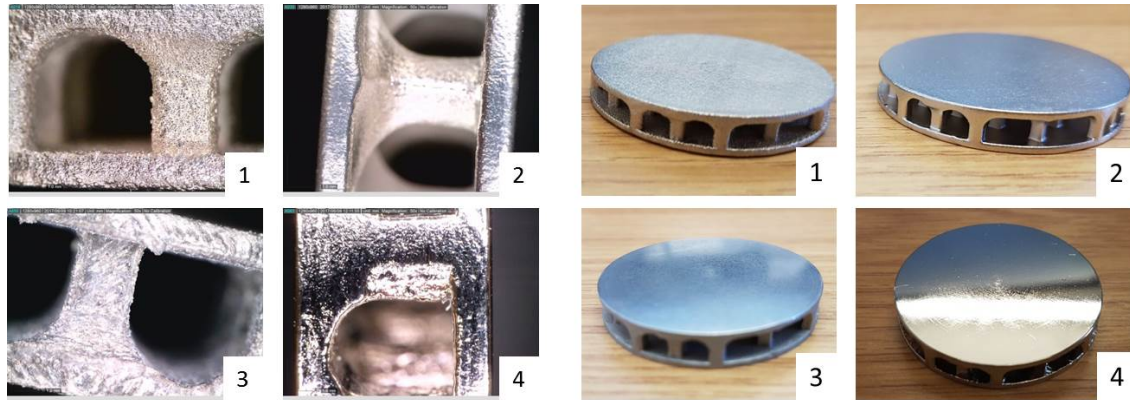
Figure 5. The four samples prior to polish: 1) glass filled nylon + Ni, 2) Bluestone + Ni, 3) aluminium and 4) aluminium + NiP

then the Ni and NiP surfaces were polished using aluminium oxide; the polishing method for the aluminium sample is proprietary. Figure 6 highlights the four polished samples, although it should be noted that the Bluestone, glass filled nylon and aluminium samples were only semi-polished as only an assessment of their ability to be polished was required.

3.1 Sample polishing - overview

The electroplated Ni on the Bluestone and glass filled nylon samples exhibited small pits within the deposit. The glass filled nylon sample was rough prior to electroplating and this required that the majority of the Ni was removed in the grinding process before a suitable surface to polish could be obtained. Figure 7(a) demonstrates how sections of the Ni were completely removed from the glass filled nylon sample, revealing the thin ($20\mu m$) copper bonding layer beneath. Previous Ni polishing at OSL demonstrated a surface roughness of $\sim$ 4nm rms on a Ni-carbon-fibre composite mirror;[9] this value provided a benchmark for the anticipated surface roughness of Bluestone and glass filled nylon samples.

The surface of the aluminium sample exhibited several deep pits as highlighted in Figure 7(b). It is suspected that these are either due to porosity within the material or from over-polishing resulting in a 'lifting' of granules from the surface. Aluminium is a soft material to polish which results in a poorer final surface quality, therefore a comparable surface quality to the nickel surfaces was not expected.

The aluminium + NiP sample was expected to demonstrate the best surface quality of the set, NiP is often used in optics fabrication and a surface roughness <1 nm rms is possible.[10] In addition, OSL has several years experience polishing the aluminium + NiP combination to a high surface quality, including in the X-ray domain.[11] One advantage of coating in NiP, or Ni, is that it removes any concern of the porosity within the printed substrate.

3.2 Surface roughness

The surface roughness of the samples was measured using the WYKO white-light microscope interferometer at OSL. A summary of the different roughness parameters are presented in Table 3, each value is an average of several measurements, although it should be noted that these values represent good quality data, as opposed to locations dominated by large pits in the case of aluminium, or visible copper in the case of glass filled nylon + Ni.

The semi-polished Ni surfaces of the Bluestone and glass filled nylon samples are similar in terms of roughness as expected. The slightly worse roughness on the glass filled nylon sample can be explained due to the excessive Ni removal required due to the initial rougher substrate. An approximate scale of the pitting that was observed in the Ni deposit can be seen in Figure 8(a). The width of the Ni pits are $\sim 50 - 30\mu m$ in diameter, in contrast the diameter of the pits from the aluminium surface are $\sim 100\mu m$ in diameter.
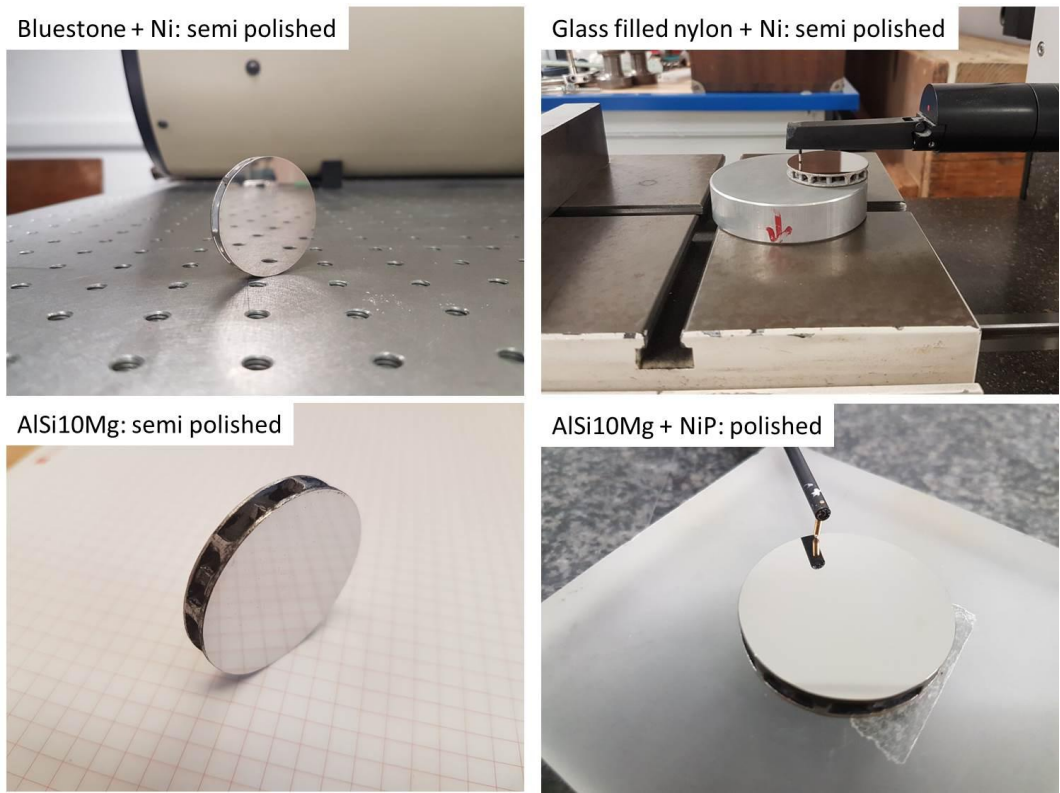
Figure 6. The four polished samples: 1) glass filled nylon + Ni, 2) Bluestone + Ni, 3) aluminium and 4) aluminium + NiP
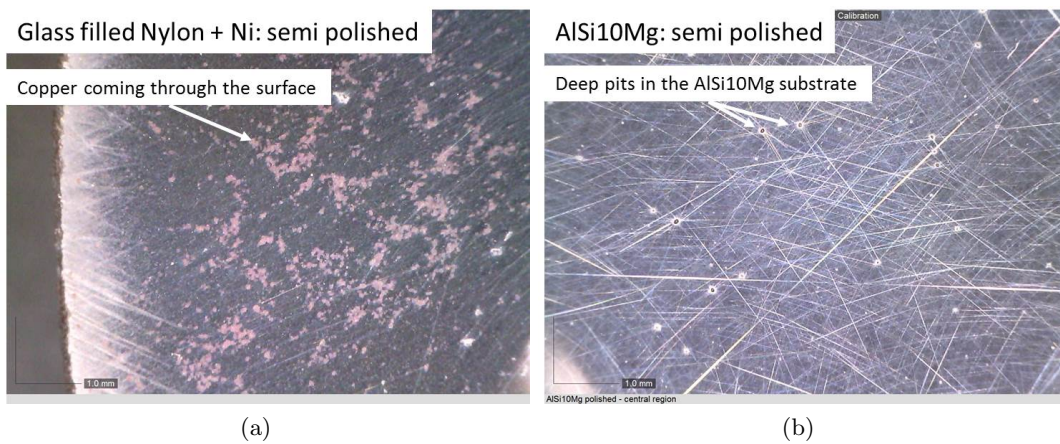

Figure 7. Microscope images highlighting the surface defects observed on the glass filled nylon sample (7(a)) and aluminium sample (7(b))

Table 3. Average surface roughness values from the four polished samples taken using the WYKO whitelight microscope interferometer

Sample	Surface roughness measurements			
	Sa [nm]	Sq [nm]	Sz [nm]	St [nm]
1. Bluestone + Ni (semi-polish)	4.51	7.29	100.47	164.14
2. Glass filled nylon + Ni (semi-polish)	5.24	7.35	87.49	180.98
3. Aluminium (semi-polish)	7.10	10.05	117.61	289.22
4. Aluminium + NiP (polish)	1.90	2.51	34.77	78.03

Sa = absolute mean, Sq = root mean squared, St = peak-to-valley (PV)
Sz = the sum of the largest peak height value and largest valley depth value
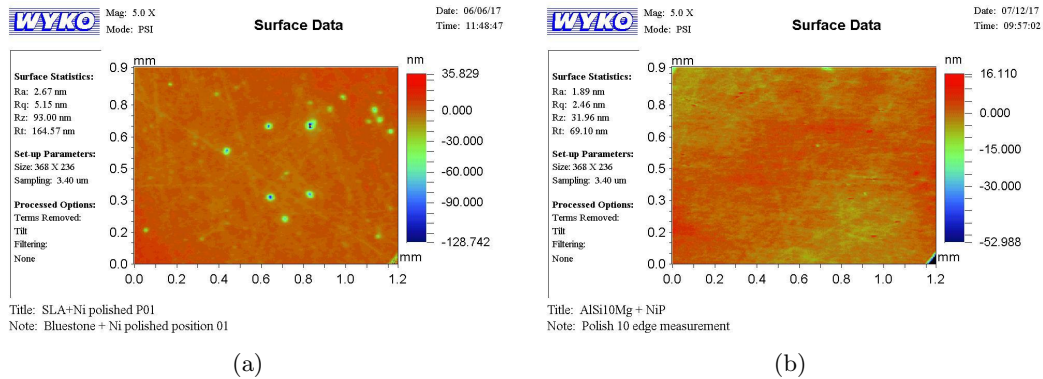within the sampling area[12]

Figure 8. WYKO white-light microscope interferometer images of the Bluestone + Ni (8(a)) and the aluminium + NiP sample (8(b))

An example of the surface texture for the aluminium + NiP sample is shown in Figure 8(b). Unlike the other three samples there is no evidence of pitting within the NiP deposit. The rms roughness (Sq) for the sample is $\sim 2.51nm$, although this is considered 'rough' for the X-ray domain, this surface finish would be defined as near precision quality at visible wavelengths. It is suspected that the peak-to-valley (St) value for the aluminium + NiP is an over-estimation caused by a series of bad pixels in the bottom right of Figure 8(b).

3.3 Surface form

The optical prescription of the samples was defined to be flat; this was specified for ease of polish and metrology. The Talysurf Intra profilometric measurements were performed in the three orientations as outlined in Section 2.2. Table 4 highlights the average form error values, in terms of PV, absolute mean and rms, for all orientations for each sample. All of the four samples exhibited a concave form post-polish and the removal of this low order term was performed using a Fourier filter with a cut-off of 10mm.

The Bluestone and glass filled nylon samples demonstrated a strongly concave form with a PV of $\sim 2.5\mu m$ and $\sim 4.2\mu m$ respectively. These values are significantly greater in magnitude than the two aluminium substrates, the explanation for this is due to less time being spent polishing these samples than the aluminium substrates. In contrast the aluminium substrates are much flatter and exhibit a PV of $< 1\lambda$ $(\lambda = 633nm)$.

Figure 9 highlights the 0° orientation data for the four samples and this data links to the low order removal data in Table 4. The Bluestone plot indicates a strong periodic feature which is likely consistent with polishing print-through effects and also demonstrates an increased roughness towards the edges of the sample. The glass filled nylon sample appears to have some localised periodic structures which possibly indicates polishing print-through; however, a lack of the continuation of the period suggests that this may not be the case.

Table 4. Analysis of form error data taken using a Talysurf Intra in 3 orientations.

Sample	All freq.	Low order removal		
	PV^b [nm]	PV^a/PV^b [nm]	$mean^a$ [nm]	rms^a [nm]
1. Bluestone + Ni (semi-polish)	2481	884/342	80	92
2. Glass filled nylon + Ni (semi-polish)	4179	1125/830	65	102
3. Aluminium (semi-polish)	519	3049/318	34	106
4. Aluminium + NiP (polish)	432	539/90	12	16

[a] - Includes all spatial frequency information
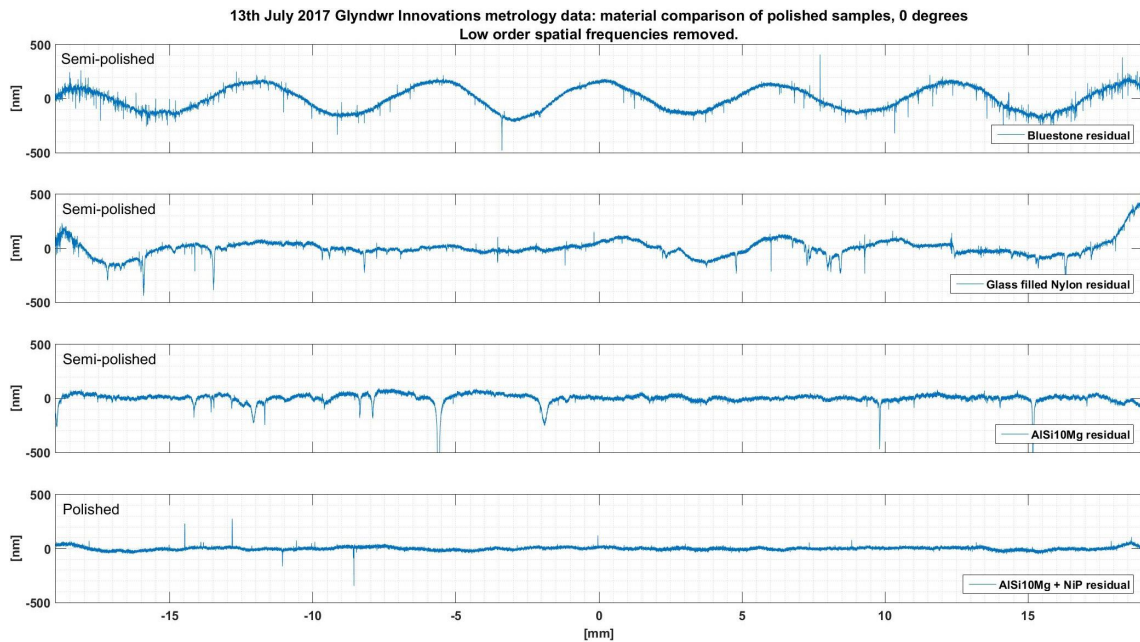[b] - Includes only form error and waviness

Figure 9. Comparison of the four $0°$ orientation datasets for each of the samples with the low-order frequencies removed.

The aluminium sample is relatively flat, but pits are dominant in the surface highlighting the rough nature of the surface. In contrast the aluminium + NiP is smooth and flat; however, upon further inspection an additional frequency is observed which has a period of $\sim 1.3mm$. The period of this artefact is inconsistent with a print-through effect and therefore it is deemed to be a polishing artefact.

3.4 Sample weights

Table 5 highlights the weight of the samples at different stages during the production process. The benefit of using the lower density materials, Bluestone and glass filled nylon, is negated when the Ni is added for the polishing layer; however, the harder surface for polishing did provide better results in terms of surface roughness than the softer aluminium substrate at a similar weight. The aluminium + NiP was significantly heavier than the other three samples, but it did demonstrate the best optical surface qualities. The weights noted for the aluminium sample suggest zero mass removal; this is known to be inaccurate and the error is likely due to two different sets of scales being used in its measure with potential error in their calibration, it is suspected that between 0.1-0.3g of material was probably removed.

Table 5. Weights of samples before and after polishing

Sample #	Post-print [g]	Post-coating [g]	Post-polish [g]
1. Bluestone + Ni	5.6	9.4	9.2
2. Glass filled nylon + Ni	4.4	8.6	8.0
3. Aluminium	9.0^a	-	9.0
4. Aluminium + NiP	9.2	14.6	14.3

^{a} - *Alternative measurement equipment was used.*

3.5 Polishing conclusion

This section has described the ability to create reflective surfaces using three different AM material combined with three different polished surfaces. The goal was to provide metrology data from which an assessment of the sample's optical surface could be made leading to a down selection for the second set of samples. Ideally further research would be undertaken to clarify the polishing print-through suspected in the glass filled nylon sample and to identify the origin of the small pits exhibited in the electroplated Ni deposit.

4. TOPOLOGY OPTIMISATION

The previous section demonstrated that it is possible to create optical surfaces using commercial additive manufacturing. Now, considering the scope that AM offers in terms of previously impossible structures, the user now has a wider design space than before. The questions becomes, *'if you can build almost any design, how do you select the best?'*

Topology optimisation is a finite element analysis tool that can be used to optimise a structural design for a given mass fraction by minimising the total internal strain energy of the system.[13–16] Figure 10 highlights the concept of topological optimisation, the left image highlights a typical CAD/FEA design where a force is applied to the top substrate and the base is fixed in x, y, and z. The image on the right highlights the resultant topological design for a 50% mass reduction.

The magnitude of the mass removal can be controlled by varying the gamma (γ) value; this is a value between 0 and 1, where 0 represents zero mass removal and 1 refers to 100% mass removal. To create the pillar structure in Figure 10, the topology optimisation penalises each element in the mesh to a value between 1 and 0 and this in turn is multiplied by the Young's modulus of the material. Therefore if $\gamma = 0.5$, 50% of the penalisation will be 1s and 50% will be 0s and in turn this will result in only 50% of the mass being equal to the material's Young's modulus (the remainder is equal to 0). Examples of how topology optimisation has previously been applied to mirror design can be seen in the papers by *Qu, Y. et al.*[17] and *Liu, J. et al.*[18]
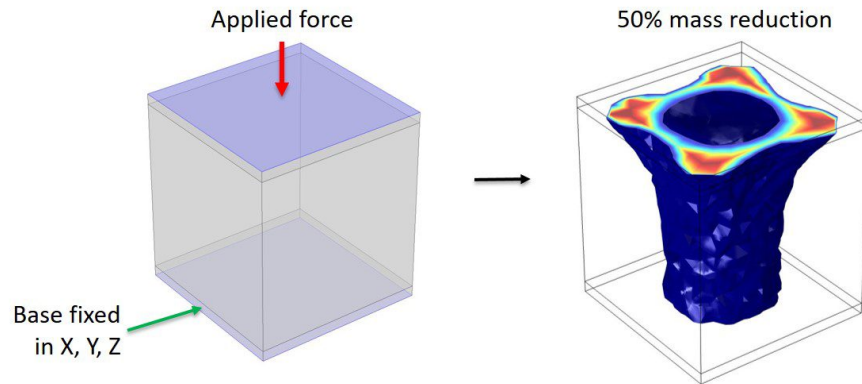
Figure 10. A schematic of the topological optimisation concept.

4.1 Second sample topological design

In the design of the second sample the thickness of the top and bottom substrates was reduced from 1mm to 0.5mm, this was done partly as a means to reduce weight, but also to bring the substrate thickness in line with the thickness of current lightweight X-ray optics.[19, 20] Topology optimisation was used to redesign the lightweighting support structure in the hope that the optimised lightweighting would help minimise the increase in polishing print-through effect caused by the reduction in substrate thickness. Figure 11 depicts how topology optimisation has been applied to the sample; γ has been decreased from 0.5 to 0.3 and the influence of this mass reduction is demonstrated in the geometry change. A ring structure is simulated when $\gamma = 0.5$ and $\gamma = 0.4$; however, at $\gamma = 0.3$ the ring structure breaks down and a 'pillar' structure is considered optimal. The pillar structure at $\gamma = 0.3$ was considered undesirable as the surface form error of the print-through effect would change depending on the measurement orientation on the optical surface. Therefore the point at which the ring structure breaks down to the pillar structure was sought. Figure 12 highlights the point at which the ring structure breaks down. It can be seen that the maximum mass removal, while maintaining a continuous ring structure, is at $\gamma = 0.38$.
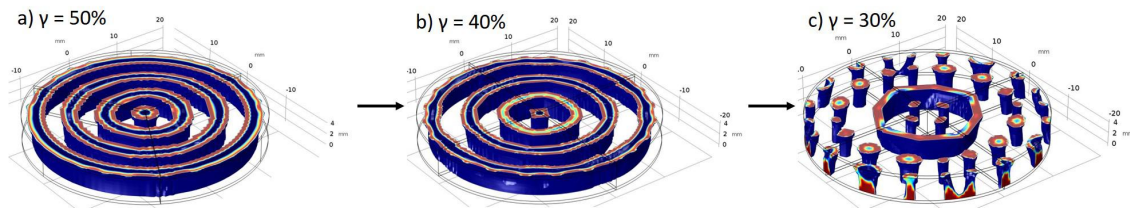

Figure 11. a) $\gamma = 0.5$, 50% of mass remaining; b) $\gamma = 0.4$, 40% of mass remaining; and c) $\gamma = 0.3$, 30% of mass remaining

5. DESIGN AND MANUFACTURE OF OPTIMISED SAMPLES.

The materials from the first study were down selected so that only two samples would be fabricated in the second round. The material combinations selected were: aluminium + NiP and Bluestone + Ni. The aluminium + NiP gave the best overall results in terms of surface roughness and form error despite being the heaviest sample. The Bluestone + Ni gave the second best surface roughness, but the best surface immediately post-build, in addition the stereolithography method was deemed a good contrast to the metal laser system of the aluminium.

The topology optimisation at $\gamma = 0.38$ was used as a template to design the new sample - Figure 13. The first iteration of the design modelled the optimisation faithfully, including the trough observed on the top of the ring supports. As shown in Figure 13, the inclusion of the trough required a design modification in order to allow the removal of the non-solidified material from the cavity - without removal of the non-solidified material the lightweighting advantage of the trough would be null and the part will potentially become a composite with
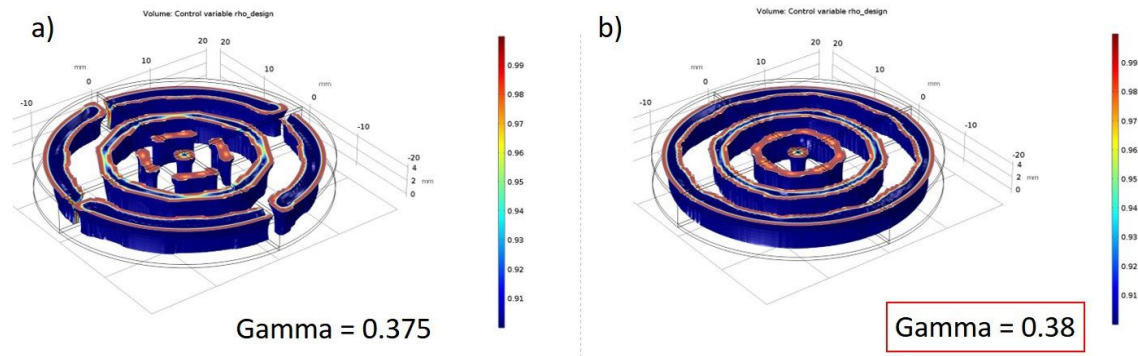
Figure 12. a) 37.5% of mass remaining - broken ring structure, b) 38% of mass remaining - complete ring structure

different material properties. Therefore access to the non-solidified material was required and achieved through the addition of narrow channels, 0.5mm in diameter, reaching from the base to the trough.
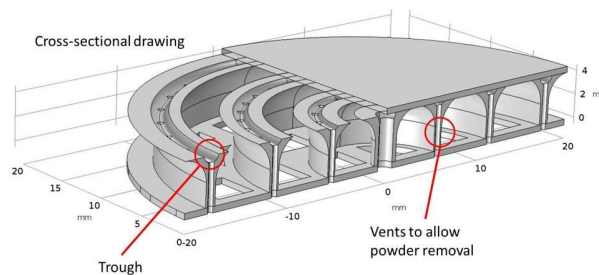

Figure 13. Preliminary design for the optimised lightweighting for the second sample.

Upon consultation with CA Models the design was deemed printable, but the narrow channels could not be fabricated without the possibility of fusion between the channel walls. It was suggested that the minimum channel diameter should be $\sim 1mm$ in diameter, but unfortunately this was approximately the width of the supports, therefore a redesign of the lightweighting structure was required.
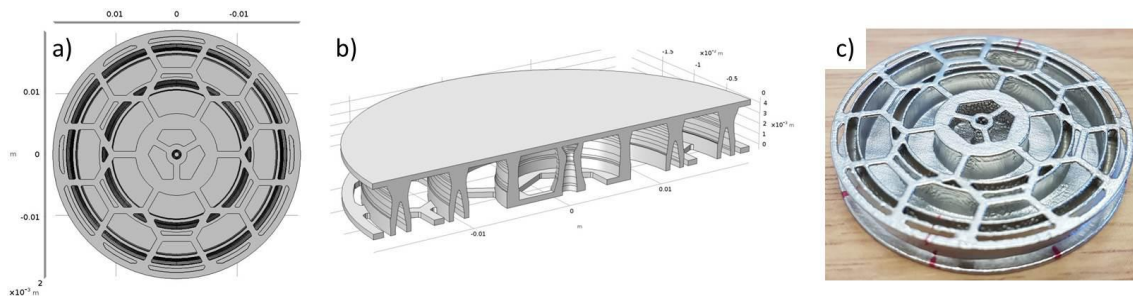

Figure 14. a) and b) highlight the initial selected design for the second sample. c) depicts the base of the post-print Bluestone + Ni sample

Figure 14 a) and b) show the redesign. The troughs are now located at the base of the structure as this allows direct access to the hollow in order to remove the non-solidified material. The base has been lightweighted to allow removal of the non-solidified material between the rings, but a secondary consideration is to allow the part to be further lightweighted as a solid base was not necessarily required.

Unfortunately when this new sample was built in the aluminium, the supports that held the sample during

build caused damage to the the thin hexagonal lightweighted base structure upon removal. Therefore a further redesign of the base was was required for the aluminium sample. The Bluestone sample however built well via the stereolithography process (Figure 14 c)). Figure 15 a) and b) depict the re-design for the aluminium sample and the successful print is shown in Figure 15 c). Only the base of the sample was altered, the lightweighting and the top remain identical to the Bluestone sample and therefore the spatial frequencies of polishing print-through should be nominally identical.
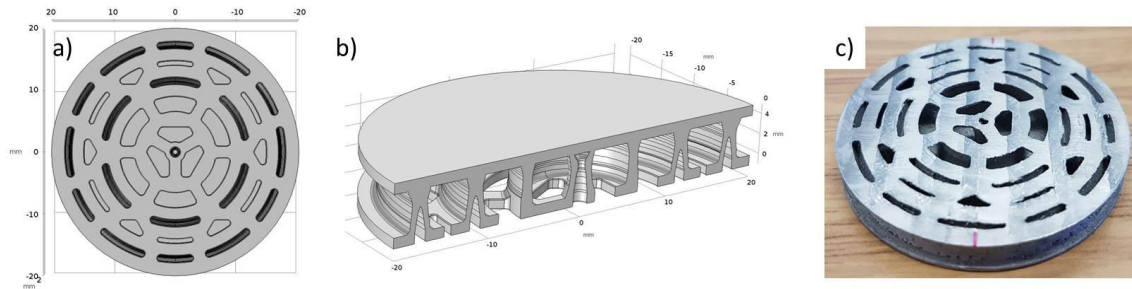

Figure 15. a) and b) highlight the redesign for the aluminium + NiP second sample. c) depicts the milled base of the aluminium sample before NiP coating

The samples depicted in Figures 14 c) and 15 c) were completed in mid August 2017 and will now undergo contact profilometry to characterise their surfaces in preparation for polishing. It is expected that a complete polish on both samples will be complete by the end of September 2017. Finally, interms of weight, The Bluestone samples before and after Ni coating were $\sim 4.2g$ and $\sim 6.2g$ respectively and the weight of the milled aluminium sample was $\sim 6.4g$. In comparison with the first set of samples this is an approximate one third weight reduction.

6. SUMMARY AND FUTURE WORK

6.1 Summary

This paper has outlined the progress made in the experimental theme of a UKSA funded project titled *'Additive manufactured space-based optics'*. One goal of the experimental theme was to use commercially available additive manufacturing capabilities to create a number of samples which were then polished to evaluate the quality of the mirror surface - this has been demonstrated in Sections 2 and 3. The second goal of the experimental theme was to investigate new lightweighting techniques and how these could be applied to a second sample design. Topology optimisation has been applied to achieve this goal and its implementation has been discussed in Sections 4 and 5.

6.2 Future work

In the immediate future of the UKSA project which is due to complete in September 2017, the new Bluestone + Ni and aluminium + NiP samples will be polished in the hope that better optical surfaces will be achieved. In parallel the theoretical theme outlined in *Feldman et al.*[2] will finalise an X-ray reflecting prototype design based on the results within this paper and if future funding should become available, the design will be fabricated and then tested at the University of Leicester X-ray tunnel test facility.

Upon completion of this project, the direction of this research will be towards materials with more suitable physical properties for optical applications, such as low CTE and higher Young's modulus. In addition, the dimensions of the samples will be increased, as it is anticipated that in doing so the stress created in the part during build may become more apparent.

REFERENCES

[1] Gaskin, J. A., "Lynx mission concept status," in [*Proc. SPIE*], **10397**(10397-29) (2017).

[2] Feldman, C. H., Atkins, C., Willingale, R., Brooks, D., Doel, P., Watson, S., and Cochrane, W., "Design and modeling of an additive manufactured thin shell for x-ray astronomy," in [*Proc. SPIE*], **10399**(10399-53) (2017).

[3] Sweeney, M., Acreman, M., Vettese, T., Myatt, R., and Thompson, M., "Application and testing of additive manufacturing for mirrors and precision structures," *Proc. SPIE* **9574**, 957406–957406–13 (2015).

[4] Herzog, H., Segal, J., Smith, J., Bates, R., Calis, J., De La Torre, A., Kim, D. W., Mici, J., Mireles, J., Stubbs, D. M., and Wicker, R., "Optical fabrication of lightweighted 3d printed mirrors," *Proc. SPIE* **9573**, 957308–957308–15 (2015).

[5] Vukobratovich, D., [*Optomechanical Engineering Handbook*], CRC Press LLC (1999).

[6] CAModels, "Data sheet - AlSi10Mg." http://www.camodels.co.uk/media/1288/metal-ad-alsi10mg.pdf.

[7] CAModels, "Data sheet - Bluestone." http://www.camodels.co.uk/media/1253/00-sla-bluestone-ready.pdf.

[8] Atkins, C., Wang, H., Doel, P., Brooks, D., Thompson, S., Feldman, C., Willingale, R., Button, T., Rodriguez Sanmartin, D., Zhang, D., James, A., and Theobald, C., "Future high-resolution x-ray telescope technologies: prototype fabrication methods and finite element analysis," in [*Society of Photo-Optical Instrumentation Engineers (SPIE) Conference Series*], **7011** (Aug. 2008).

[9] Thompson, S. J., Brooks, D., and Doel, A. P., "A nickel-carbon-fibre composite for large adaptive mirrors: fabrication methods and properties," *Opt. Express* **16**, 1321–1330 (Jan 2008).

[10] Schwertz, K. and Burge, J. H., [*Field Guide to Optomechanical Design and Analysis*], CRC Press LLC (2012).

[11] Atkins, C., Wang, H., Doel, P., Brooks, D., Thompson, S., Feldman, C., Willingale, R., Button, T., Rodriguez Sanmartin, D., Zhang, D., James, A., Theobald, C., Willis, G., and Smith, A. D., "Active x-ray optics for the next generation of x-ray telescopes," in [*Society of Photo-Optical Instrumentation Engineers (SPIE) Conference Series*], **7360** (May 2009).

[12] Leach, R., Brown, L., Jiang, X., Blunt, R., Conroy, M., and Mauger, D., [*Guide to the Measurement of Smooth Surface Topography using Coherence Scanning Interferometry*], National Physical Laboratory (2008).

[13] COSMOLMultiphysics, "Topology Optimization of an MBB Beam." https://www.comsol.com/model/topology-optimization-of-an-mbb-beam-7428.

[14] Loubet, B. and COSMOLMultiphysics, "Finding a Structure's Best Design with Topology Optimisation." https://www.comsol.com/blogs/finding-a-structures-best-design-with-topology-optimization/ (2015).

[15] COSMOLMultiphysics, "Topology Optimization of a Loaded Knee Structure." https://www.comsol.com/model/topology-optimization-of-a-loaded-knee-structure-4374.

[16] Carver, L. and COSMOLMultiphysics, "Virtual Material Design in 3D Printing Makes Headway with Multiscale Modeling." https://www.comsol.com/story/virtual-material-design-in-3d-printing-makes-headway-with-multiscale-modeling-35871.

[17] Qu, Y., Wang, W., Liu, B., and Li, X., "Topology optimization design of space rectangular mirror," *Proc. SPIE* **10154**, 1015421–1015421–7 (2016).

[18] Liu, J. and Jiang, B., "Topology optimization design of a space mirror," *Proc. SPIE* **9795**, 97952Y–97952Y–10 (2015).

[19] Riveros, R. E., Biskach, M. P., Allgood, K. D., Mazzarella, J. R., Sharpe, M. V., and Zhang, W. W., "Progress on the fabrication of high resolution and lightweight monocrystalline silicon x-ray mirrors," *Proc.SPIE* **9905**, 9905 – 9905 – 5 (2016).

[20] Proserpio, L., Wen, M., Breunig, E., Burwitz, V., Friedrich, P., and Madarasz, E., "Indirect slumping of d263 glass on fused silica mould," *Proc.SPIE* **9905**, 9905 – 9905 – 8 (2016).